Translational and internal states of hydrogen molecules produced from the ultraviolet photodissociation of amorphous solid methanol

Tetsuya Hama, Masaaki Yokoyama, Akihiro Yabushita, and Masahiro Kawasaki[a)]
Department of Molecular Engineering, Kyoto University, Kyoto 615-8510, Japan

(Received 28 July 2008; accepted 27 February 2009; published online 23 April 2009)

Translationally and internally hot H_2 molecules are produced from the 157 nm photodissociation of amorphous solid methanol at 90 K by two distinct mechanisms: exothermic recombination of two H-atom photoproducts bound to the surface and unimolecular molecular elimination of H_2 from the photoexcited methanol. The vibrationally hot $H_2(v=2-5)$ products are characterized by high translational and rotational temperatures. A third mechanism, the almost thermoneutral abstraction of a hydrogen atom from methanol parent molecule by the photolytically produced hydrogen atom, yields translationally and rotationally cold H_2 ($v=0$ and 1) products. Comparison with the results of the vacuum ultraviolet photolysis of water ice is discussed. Production of translationally hot and cold hydrogen atoms is also confirmed. © *2009 American Institute of Physics*.
[DOI: 10.1063/1.3100961]

I. INTRODUCTION

Molecular hydrogen is the most abundant molecular species in the interstellar medium and is thought to be produced mostly via surface reactions on interstellar grains and to a lesser extent via photochemical processes on ice covered surfaces of comets, planets, and dust grains.[1] Dust grains in molecular clouds at temperatures below ~130 K are covered with an amorphous water ice mantle, which is irradiated by vacuum ultraviolet light (VUV) light. Hot and cold molecular hydrogen can then be formed by photodissociation of water molecules and the subsequent reaction of the H-atom photoproducts with either other H atoms or the ice matrix, respectively. The efficiency of H_2 formation via this photodissociation has been discussed.[2,3] Methanol is typically observed within water rich interstellar ices.[4] Because its abundance in some grain mantles varies between 0.05 and 0.50 relative to water,[5,6] photolysis of methanol may also be a source of interstellar hydrogen.

The internal energy distribution is a key parameter for all interstellar chemistry because hot species enable chemical reactions that are not possible when the species are in their ground states. For example, the rate constant for the $O(^3P)+H_2(v=3)$ reaction at 100 K is predicted to be about 11 orders of magnitude larger than that for $H_2(v=0)$ according to a theoretical calculation.[7] Molecular dynamics calculations were performed for the hydrogen recombination mechanism on an amorphous solid water surface at 70 K, and the formation of translationally excited H_2 in a broad range of the vibrational levels, $3 \le v \le 12$, peaking at $v=9$ was predicted by Takahashi.[8] In experimental studies, the formation of hydrogen molecules from the recombination reaction of hydrogen atoms on amorphous water ice at 10 K was reported by Roser *et al.*,[9] and vibrationally excited HD (up to $v=7$) formed on a graphite surface via the recombination reaction at 15 K was detected by Price and co-workers.[10–12] There have been several experiments on the formation of H_2 by photolysis of amorphous water ice.[13–15] Westley *et al.*[14] and Watanabe *et al.*[15] estimated the H_2 formation efficiencies but did not report on details such as the reaction mechanisms or the energy partitioning in the reaction products. Recently, Yabushita *et al.* reported the production of H atoms and H_2 molecules from the photodissociation of amorphous solid water at 100 K.[3,16,17] Their results showed that (a) the vibrational population is represented by two distinct distributions: one peaks at $H_2(v=0)$ and the other increases with increasing vibrational quantum number for $H_2(v=2-5)$, (b) hydrogen abstraction from H_2O by a photolytically produced hot H atom yields mainly $H_2(v=0)$ and to a small extent $H_2(v=1)$, and (c) hydrogen recombination of two H-atom photoproducts yields $H_2(v \ge 2)$. For these H_2 products, the ortho/para ratio g_{OPR} was 3, which is a useful indicator for the physical and chemical history of H_2 in interstellar clouds. The mechanisms are shown schematically in Fig. 1, and energetics of the H_2 formation by water ice photolysis is summarized as follows:

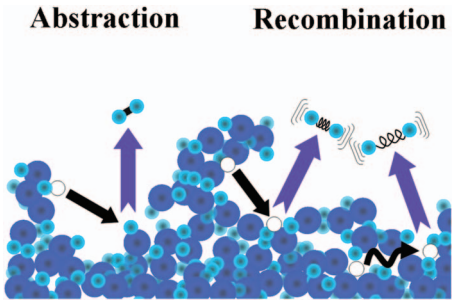

FIG. 1. (Color) Schematic illustrations of the hydrogen atom abstraction and hydrogen atom recombination mechanisms for forming vibrationally cold and hot H_2 during VUV irradiation of amorphous solid water. White balls represent photolytically produced hot H atoms.

[a)]Author to whom correspondence should be addressed. Electronic mail: kawasaki@photon.mbox.media.kyoto-u.ac.jp. FAX: +81-75-383-2573.

	ΔH	E_a(kcal/mol)	
$H_2O \rightarrow H + OH$,	118	–	(1)
$H + H \rightarrow H_2$,	− 104	0	(2)
$H + HOH \rightarrow H_2 + OH$.	14	23	(3)

Here, ΔH is the standard heat of reaction and E_a is the activation energy of the respective reaction in the gas phase.

In the solid phase photolysis of methanol at low temperature, one expects that the same two mechanisms for H_2 formation are important, i.e., highly exothermic hydrogen atom recombination (HR) and almost thermoneutral hydrogen atom abstraction (HAB). In addition one needs to consider unimolecular hydrogen molecule elimination (UMHE) reaction. The energetics for the respective reactions of methanol in the gas phase are summarized as follows:[18,19]

		ΔH	E_a(kcal/mol)	
	$CH_3OH \rightarrow CH_3O + H$,	104	–	(4)
	$CH_3OH \rightarrow CH_2OH + H$,	92	–	(5)
UMHE:	$CH_3OH \rightarrow CHOH + H_2$,	71	–	(6)
UMHE:	$CH_3OH \rightarrow CH_2O + H_2$,	19	–	(7)
HR:	$H + H \rightarrow H_2$,	− 104	0	(8)
HAB:	$H + CH_3OH \rightarrow CH_2OH + H_2$,	− 8	9	(9)
HAB:	$H + CH_3OH \rightarrow CH_3O + H_2$.	1	14	(10)

Gerakines *et al.* reported the VUV photolysis of solid CH_3OH at 10 K.[20] They suggested that (a) H_2 and H_2CO are produced directly from methanol photodissociation via reaction (6) and (b) H_2 and CH_2OH are formed via reaction (9) as a secondary process.

In this paper we have investigated the mechanisms and dynamics of H_2 production from the 157 nm photodissociation of amorphous solid methanol (ASM) at 90 K based on the direct measurement of translational energy distributions and internal states of the H_2 products that are directly detected with the resonance-enhanced multiphoton ionization (REMPI) technique.

II. EXPERIMENTAL

A. Apparatus and preparation of ice films

Surface photodissociation of ASM at 90 K was carried out by pulsed laser photolysis of the sample, which was supported on a temperature controlled cold finger in a high vacuum chamber. The experimental details are described elsewhere.[21] In brief, a vacuum chamber was evacuated to a base pressure of 10^{-8} Torr using two turbomolecular pumps in tandem (Shimadzu, 800 and 50 l s^{-1}). An optically flat sapphire substrate, sputter coated with a thin polycrystalline film of Au(111), was supported in the center of the chamber by a liquid-nitrogen-cooled manipulator connected to an *X-Y-Z* stage.[22] The temperature of the substrate was controlled to within 1 K. The temperature controller was composed of an alumel-chromel resistance thermometer with cooling by liquid nitrogen and heating from a 0.35 mm diameter tantalum filament attached to the substrate. CH_3OH and CD_3OH (98.5% D) were purchased from Wako Chemicals. ASM was prepared with the backfilling deposition of methanol vapor onto the substrate at 90 K for 60 min by a pulsed nozzle (General Valve) at a rate of 10 Hz and at 30 Torr stagnation pressure of methanol. In order to evenly distribute methanol vapor in the chamber, a flat plate was attached in front of the pulsed nozzle. The exposure was typically 1800 L (1 L$=1\times10^{-6}$ Torr s). To check the influence of residual gas on the ASM structure, the time-of-flight (TOF) spectra were measured as a function of exposure time to vacuum (10^{-8} Torr). No appreciable difference in the TOF spectra of H_2 was observed after 5 h exposure of the ASM to vacuum. Crystallization of solid methanol occurs at 103.4 K.[23]

Unfocused 157 nm laser (Lambda Physik, OPTexPro) radiation was incident at an angle of about 80° to the surface normal on the ice surface at a fluence <0.1 mJ cm^{-2} $pulse^{-1}$. It is unlikely that multiphoton process occurred with this low laser intensity.[17,24] H_2 products were subsequently ionized at a distance of 2 mm from the substrate surface by (2+1) REMPI via the $E/F\ ^1\Sigma_g^+ \leftarrow X\ ^1\Sigma_g^+$ ($v'=0$, $v''=0-5$) transition and collected with a small mass spectrometer aligned perpendicular to the ice surface. Radiation at 201–260 nm was produced by a Nd^{3+}:YAG pumped dye laser (Lambda Physik, SCANmate), with subsequent frequency doubling and mixing in KDP and BBO crystals. The delay t between the photolysis and REMPI laser pulses was varied with a delay generator to allow investigation of the flight times of the product H_2 molecules. The (2+1) REMPI detection of H(D) atom products was also performed at 243.124 (243.058) nm. The REMPI wavelength was scanned over the Doppler width for the H (D) atoms.

B. Simulation of time-of-flight spectra of H_2 products and REMPI transition factors

The measured TOF spectra were fitted with one or more flux-weighted Maxwell–Boltzmann (MB) distributions defined by a translational temperature T_{trans}. Details regarding the simulation of such TOF spectra have been reported previously.[21] The TOF spectrum $S(a_i,t,T_i)$ was fitted with a combination of the MB distributions defined by the temperature T_i. The coefficient a_i is used for relative population of each MB distribution,

$$S(a_i,t,T_i) = \sum a_i S_{\mathrm{MB}}(t,T_i), \tag{11}$$

$$S_{\mathrm{MB}}(t,r) = r^3 t^{-4} \exp[-mr^2/(2k_B T_{\mathrm{trans}} t^2)], \tag{12}$$

$$P_{\mathrm{MB}}(E_t) = (k_B T_{\mathrm{trans}})^{-2} E_t \exp[-E_t/(k_B T_{\mathrm{trans}})], \tag{13}$$

where r is the flight distance of the photofragment. The MB distribution $P_{\mathrm{MB}}(E_t)$ as a function of translational energy E_t is characterized by the averaged translational energy $\langle E_t \rangle$

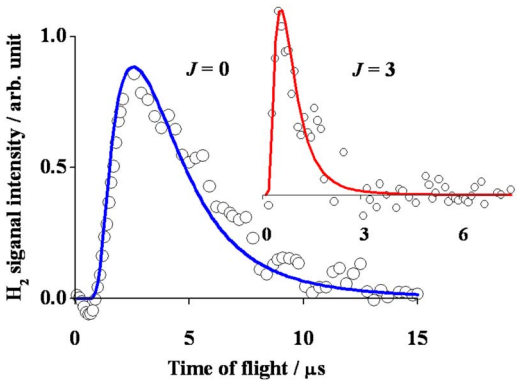

FIG. 2. (Color online) A TOF spectrum of $H_2(v=0,\ J=0)$ products from 157 nm photolysis of amorphous solid methanol. Substrate temperature =90 K. The solid line is a best fit to the data derived from assuming a MB distribution with $T_{trans}=100$ K. The inset is a TOF spectrum of $H_2(v=0,\ J=3)$ with $T_{trans}=2200$ K.

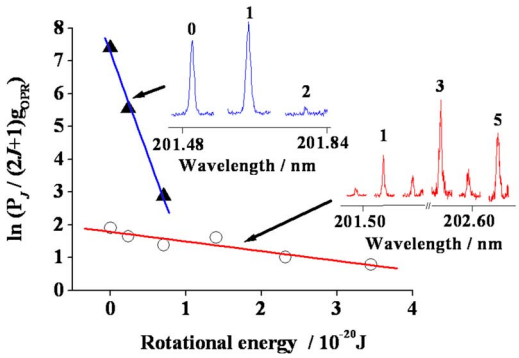

FIG. 3. (Color online) Rotational populations of $H_2(v=0)$ recorded at TOF, $t=0.55$ μs (open circle) and 3.5 μs (filled triangle). P_J is the normalized population of a rotational state. The ortho/para ratio g_{OPR} is 3. The rotational distribution recorded at $t=0.55$ μs is approximated with $T_{rot}=2500$ K, while the rotational population recorded at $t=3.5$ μs is fitted with $T_{rot}=110$ K. The insets are the REMPI spectra for $E/F(v'=0,\ J')\leftarrow X(v''=0,\ J'')$ transition of $H_2(v=0)$ products recorded at $t=0.55$ and 3.5 μs. Rotational quantum numbers J are shown above selected peaks.

$=2k_BT_{trans}$, where k_B is the Boltzmann constant. To obtain the rotational-vibrational populations $P_J(v)$, the REMPI signals measured at a constant laser power were corrected by the respective line strength factors. This line strength factor depends on the probability of the REMPI transitions, $|M_{fo}|^2$. Pomerantz *et al.* calculated $|M_{fo}|^2$ for the $E,F(v'=0,\ J'=J'')$-$X(v'',\ J'')$ (2+1) REMPI transitions in H_2 for different rovibrational levels in the X state ($0\leq v''\leq 4$, $0\leq J''\leq 21$ and $v''=5$ and 6, $J''=0$).[25] These calculations showed that the value of $|M_{fo}|^2$ varies significantly with v'' but is not strongly affected by changes in J''. We have extended the conclusions and tendencies for J'' in different v'' states on a common scale and estimated $|M_{fo}|^2$ from different rovibrational levels in the X state ($v''=5$, $0\leq J''\leq 17$) via $E,F(v'=0,\ J'=J'')$ according to Latimer *et al.*[12] All rotational data for H_2 products are consistent only with the statistical weight parameter for ortho/para hydrogen, $g_{OPR}=3$. Use of $g_{OPR}=1.3$ that would be appropriate for H_2 in thermal equilibrium at 90 K (Ref. 26) results in ragged rotational distributions that cannot be described by smooth lines or curves.

III. RESULTS

A. Formation of molecular hydrogen

1. $H_2(v=0,1)$ *from* CH_3OH

Hydrogen molecules in the vibrationally ground state $H_2(v=0,J)$ were detected, which are characterized by two different translational temperatures. The TOF spectrum for $H_2(v=0,\ J=0)$ in Fig. 2 is reproduced by a MB distribution with $T_{trans}=100\pm 10$ K. The inset in Fig. 2 shows the TOF spectrum of $H_2(v=0,\ J=3)$, which is characterized by $T_{trans}=2200\pm 300$ K. Figure 3 shows the rotational populations for $J=0$, 1, and 2 of the $H_2(T_{trans}=100$ K, recorded at $t=3.5$ μs) and for $J=0$–5 of the $H_2(T_{trans}=100$ K, recorded at $t=0.55$ μs) The rotational distributions are approximated by the Boltzmann distributions with $T_{rot}=110\pm 20$ K and $T_{rot}=2500\pm 300$ K, respectively. The translational and rotational energies of $H_2(v=0,\ J)$ and the measured population ratios are summarized in Table I. The averaged translational and rotational energies of the $H_2(v=0)$ photoproducts are calculated as $\langle E_{trans}(v=0)\rangle=0.9$ and $\langle E_{rot}(v=0)\rangle=0.5$ kcal/mol (Table II). Essentially the same results were obtained for vibrationally excited $H_2(v=1,\ J)$ although the signal intensities for $H_2(v=1,\ J)$ were much weaker than for $H_2(v=0,\ J)$.

2. $H_2(v=2,3,4$ and $5)$ *from* CH_3OH

TOF spectra of $H_2(v=2$–$5,\ J)$ are characterized by four different translational temperatures. For example, the TOF spectra for $H_2(v=3,\ J=3$ and 13) are reproduced by a combination of four MB distributions: $T_{trans}=5000\pm 1000$, 1800 ± 200, 700 ± 100, and 100 ± 10 K as shown in Fig. 4.

TABLE I. Translational and rotational temperatures and energies of $H_2(v=0)$.

	Rotational level (J)	Translational temperature T_{trans} (K)	Translational energy (kcal/mol)
	0	100 ± 10	0.4 ± 0.04
	3	2200 ± 300	8.8 ± 1.2
TOF component contributions	Rotational level (J)	Rotational temperature T_{rot} (K)	Rotational energy (kcal/mol)
$H_2(T_{trans}=100$ K, 93%)	0-2	110 ± 20[a]	0.2 ± 0.04
$H_2(T_{trans}=2200$ K, 7%)	0-5	2500 ± 300[b]	5.0 ± 0.6

[a]Signal recorded at time of flight=3.5 μs.
[b]Signal recorded at time of flight=0.55 μs.

TABLE II. Vibrational distribution and averaged translational and internal energies of $H_2(v)$.

v	Vibrational population ratio[a]	Averaged energy (kcal/mol)		
		Vibrational	Translational	Rotational
0	[b]	0	0.9	0.5
2	0.4	23.1	4.2	9.8
3	1	33.7	4.4	9.5
4	1.5	43.6	4.4	7.9
5	3.4	52.9	9.2	7.7

[a]Relative to $v=3$ for the sum over J (odd)$=1,3,\ldots,13$. Error bars are 15%.
[b]Relative population was not measured because of different experimental setups.

The rotational levels were observed up to $J=17$ as shown in Fig. 5, which were recorded at $t=0.55$ μs for the $H_2(T_{trans}=5000$ and 1800 K) and at $t=3.5$ μs for the $H_2(T_{trans}=700$ and 100 K). Figure 6 shows Boltzmann plots for the rotational populations. The translational and rotational energies of the $H_2(v=3)$ products are summarized in Table III. Essentially the same rotational distributions were observed for $H_2(v=2-5)$ as shown in Fig. 7. The averaged translational and internal energies are summarized in Table II. The vibrational distribution for $H_2(v=2-5)$ in Table II was estimated as follows: the TOF spectra were measured for $v=2-5$, $J=1-15$ (total of 60 levels) and integrated to obtain the total TOF intensity associated with each (v,J) level. The measured signal intensity for each J level was then corrected with the use of the REMPI transition probability.

3. Molecular hydrogen isotopomers from CD_3OH

The HD, D_2, and H_2 products characterized by $T_{trans}=100$ K in the rovibrational levels $(v=0,\ J=0,1,2)$ were also detected from the photodissociation of amorphous solid CD_3OH at $t=3.5$ μs. At $t=0.55$ μs, the HD in the rovibrational levels $(v=0,\ J=0-5)$ was observed; however, the signal intensities were too weak to characterize the translational temperatures. D_2 and H_2 products in the $v=0$ level were below the detection limit at $t=0.55$ μs.

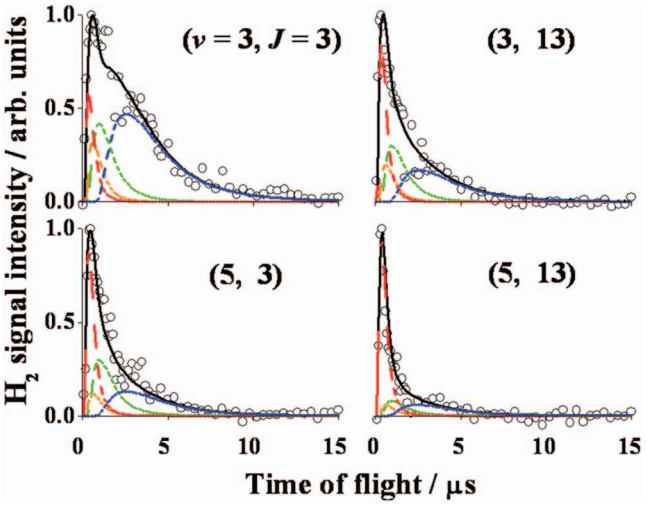

FIG. 4. (Color) TOF spectra of $H_2(v=3,\ J=3,13)$ and $H_2(v=5,\ J=3,13)$. These spectra are composed of four MB distributions with $T_{trans}=5000$, 1800, 700, and 100 K.

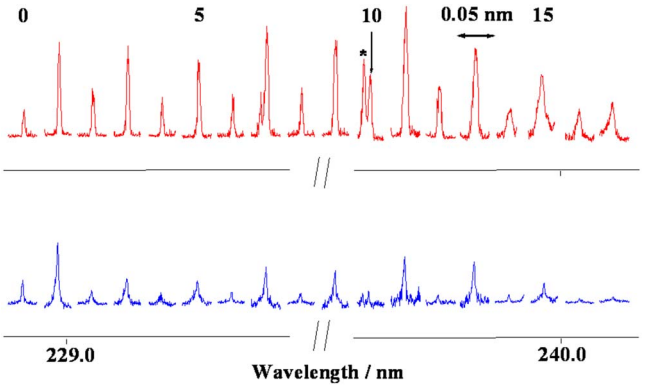

FIG. 5. (Color online) REMPI spectra for the $E/F(v'=0,\ J')\leftarrow X(v''=3,\ J'')$ transition of H_2 recorded at $t=0.55$ μs (upper panel) and 3.5 μs (lower panel). Rotational quantum numbers J'' are shown above selected peaks. The asterisk denotes an unassigned signal.

The HD, D_2, and H_2 in the rovibrational levels $(v=3,\ J=0-15)$ were measured at $t=0.55$ μs. The TOF spectrum of $H_2(v=3,\ J=13)$ is reproduced by two MB distributions with $T_{trans}=1800\pm300$ and 100 ± 10 K. The relative populations of the isotopomers in various (v,J) levels and the translational temperatures in the $(v=3,\ J=3)$ level are listed in Table IV.

B. Formation of atomic hydrogen from CD_3OH

Figure 8 shows the TOF spectrum of H-atom products from the photodissociation of CD_3OH, which is composed of three MB distributions with $T_{trans}=6000\pm1000$, 700 ± 100, and 100 ± 20 K. The inset of Fig. 8 shows the TOF spectrum of D atom products from CD_3OH, which is composed of MB distributions with the same T_{trans} as for the H-atom products. The ratio of the total signal intensities for D product/H product was 0.23 ± 0.03. Table V summarizes these results.

IV. DISCUSSION

Photodynamics and reaction mechanisms of methanol ice photolysis are similar to those described previously for

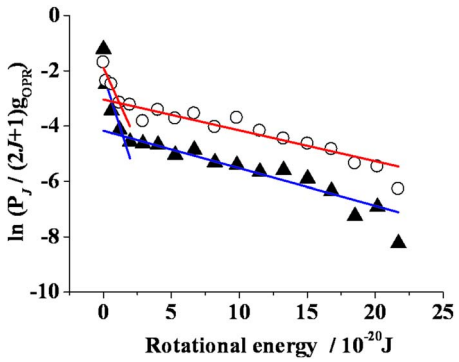

FIG. 6. (Color online) Rotational state populations of $H_2(v=3)$ recorded at $t=0.55$ μs (open circle) and 3.5 μs (filled triangle). The rotational distribution at $t=0.55$ μs for $J\leq3$ is approximated with $T_{rot}=670$ K. The population for $5\leq J\leq16$ is fitted with $T_{rot}=6500$ K. The rotational population recorded at $t=3.5$ μs is fitted with $T_{rot}=470$ K for $J\leq3$ and 5400 K for $5\leq J\leq16$.

TABLE III. Translational and rotational temperatures and energies of $H_2(v=3)$.

	Rotational level (J)	Translational temperature T_{trans} (K) and contribution (%)	Averaged translational energy (kcal/mol)
	3	5000 (10%), 1800 (10%), 700 (20%), 100 (60%)	3.5 ± 0.6
	13	5000 (25%), 1800 (10%), 700 (25%), 100 (40%)	6.5 ± 1.2
TOF components	Rotational level (J)	Rotational temperature T_{rot} (K)	Averaged rotational energy (kcal/mol)
$H_2(T_{trans}=700$ and 100 K)	0-3	470 ± 100[a]	8.7 ± 1.4
	5-16	5400 ± 500[a]	
$H_2(T_{trans}=500$ and 1800 K)	0-3	670 ± 100[b]	10.8 ± 1.7
	5-16	6500 ± 400[b]	

[a]Signal recorded at time of flight=3.5 μs.
[b]Time of flight=0.55 μs.

water ice photolysis.[16,17] Therefore, first we describe the H and H_2 production mechanisms from amorphous solid water and then discuss the results for ASM.

A. Relaxation and reactions of hydrogen atoms

1. Hydrogen atoms from the vacuum ultraviolet photolysis of water ice

Yabushita *et al.* reported the TOF spectrum of H atoms released following photoexcitation of amorphous solid water film at 100 K,[17]

$$H_2O + h\nu \rightarrow \text{hot-H} + OH\,. \qquad E_{avail}(\text{kcal/mol}) = 63 \qquad (14)$$

E_{avail} is the maximum available energy in the 157 nm photolysis of gaseous water. Three MB components were required to fit the TOF spectrum measured at 157 nm: T_{trans} =4750 (3%), 625 (5%), and 110 (92%) K. Table V summarizes the translational temperatures and contributions of each component. These results may be understood by recognizing that H atoms will be produced mostly in the bulk phase as well as from the exposed surfaces within the porous amorphous solid water film. Yabushita *et al.* attributed the H atoms (T_{trans}=4750 K) released without collisions into vacuum, which are atomic photoproducts formed by photodissociation of the uppermost H_2O layer of the ice film either within the pore structures or directly at the ice-vacuum interface. The H atoms (T_{trans}=625 and 110 K) are attributed to the photodissociation of water molecules in the deeper monolayers.[17] Andersson *et al.* reported that the energy transfer efficiency between a H atom and the center-of-mass motion of a H_2O molecule in water ice is 0.2.[27] The H atoms (T_{trans}=4750 K) then require eight to ten collisions to reduce their translational energy to T_{trans}=625 K and need eight to ten more collisions to thermally equilibrate to T_{trans}=110 K. As the distance from the surface monolayer increases, the fraction of H atoms that succeeds in escaping from the surface is expected to decline; most H atoms arising from photolysis of such embedded molecules recombine to form H_2 via the HR mechanism (2) or induce an abstraction reaction to form H_2 via the HAB mechanism (3) as shown in Figs. 9(a) and 9(b).

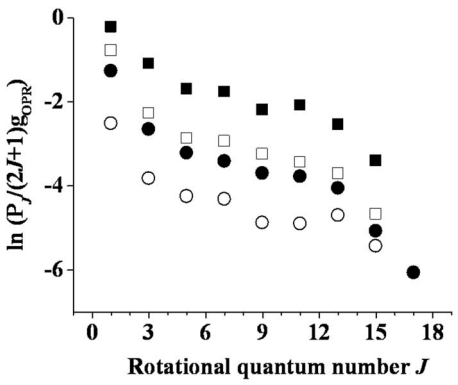

FIG. 7. Rotational population distributions associated with different $H_2(v)$, obtained from integrated TOF spectra: v=2 (○), 3 (●), 4 (□), and 5(■).

2. Hydrogen atoms from the vacuum ultraviolet photolysis of amorphous solid methanol

The elimination reactions of the methyl hydrogen atom and the hydroxyl hydrogen atom from the 157 nm photolysis of CH_3OH are

$$CH_3OH + h\nu \rightarrow CH_3O + \text{hot-H}, \qquad E_{avail}(\text{kcal/mol}) = 77 \qquad (15)$$

$$\rightarrow CH_2OH + \text{hot-H}\,. \qquad 89 \qquad (16)$$

Since the translational energies of H(D) atoms from photolysis of CD_3OH are found to be much lower than the maximum available energy E_{avail} associated with reactions (4) and (5) as shown in Table V, we propose that the nascent hydrogen products are relaxed by collisions within the ASM matrix as described above for amorphous solid water. These H atoms are produced in the deeper monolayers of ASM. If we assume that the hydrogen atoms (T_{trans}=6000 K, 30% for H and 45% for D in Fig. 8 and Table V) are the nascent products from the surface CD_3OH, the ratio of the methyl hydrogen atom elimination over the hydroxyl hydrogen atom elimination may be estimated to be $(0.23 \pm 0.03) \times (0.45/0.30) = 0.35 \pm 0.05$ from the total signal intensity ra-

TABLE IV. Relative populations and translational temperatures of HD, D_2, and H_2 from photoreactions of CD_3OH.

	Rovibronic level (v,J)						T_{trans} (K) and contribution (%) of HD, D_2, and H_2 in the level of $v=3$ and $J=3$
	(2,3)	(3,3)	(3,13)	(3,14)	(4,3)	(0,0)[a]	
HD	0.71	0.53	0.61	0.47	0.69	0.60	5000 (15%), 700 (35%), 100 (50%)
D_2	0.16	0.27	0.24	0.47	0.21	0.32	1800 (25%), 100 (75%)
H_2	0.13	0.20	0.15	0.06	0.10	0.08	1800 (20%), 100 (80%)

[a]Translational temperatures of HD, D_2, and H_2 ($v=0$, $J=0$) are 100 ± 10 K.

tio (D/H) corrected for the nascent population ratio. The elimination ratio in the gas phase was reported to be 0.5.[28] The reaction mechanisms for CD_3OH are summarized as follows:

Yield ratio

$$CD_3OH + h\nu \rightarrow \text{hot-H} + CD_3O, \qquad 1$$

$$CD_3OH + h\nu \rightarrow \text{hot-D} + CD_2OH, \qquad 0.35 \pm 0.05$$

$$\text{H and D } (T_{trans} = 6000 \text{ K}) \xrightarrow{\text{collision}} \text{H and D (700 K)},$$

$$\text{H and D (700 K)} \xrightarrow{\text{collision}} \text{H and D (100 K)}.$$

The comparison with the hydrogen atoms photogenerated from amorphous solid water is shown in Table V. The average translational energy of hydrogen atoms from CD_3OH is higher than that from amorphous solid water because the excess energies of reactions (4) and (5) are larger than that of reaction (1). Since the activation energies of reactions (9) and (10) are smaller than that of reaction (3), a larger fraction of hydrogen atoms from ASM photolysis can react with the bulk methanol on collision rather than thermally equilibrate and desorb. Figures 9(c) and 9(d) show schematics illustrating the H-atom reaction processes in the ASM photoreaction.

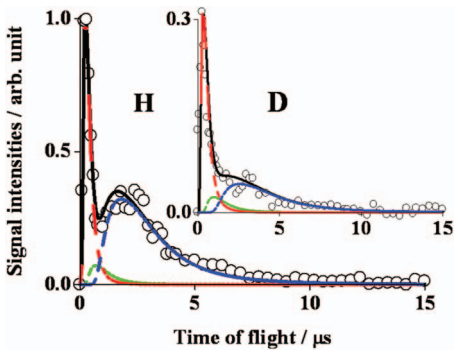

FIG. 8. (Color) A TOF spectrum of H atoms from the 157 nm photolysis of solid amorphous CD_3OH at 90 K. This spectrum is composed of three MB distributions with $T_{trans}=6000$ K (30%), 700 K (5%), and 100 K (65%). The inset is a TOF spectrum of D atoms. The solid curves are best fits with $T_{trans}=6000$ K (45%), 700 K (10%), and 100 K (45%).

B. Formation mechanisms of vibrationally cold and hot hydrogen molecules

1. Hydrogen molecules in v=0 and 1 levels

a. Amorphous solid water We have previously reported the $H_2(v=0-4)$ formation mechanisms from the 157 nm photodissociation of amorphous solid water. $H_2(v=0, J=0-2, T_{trans}=100$ K, $T_{rot}=100$ K, 96% contribution) component was formed in the bulk as well as from the exposed surfaces within the porous ice film via the HAB reaction (3), while $H_2(v=0, J=1-5, T_{trans}=1500$ K, $T_{rot}=1300$ K, 4%) was produced very near the amorphous solid water/vacuum interface.[3,16] $H_2(v=1)$ was formed but its population was very small. The HAB reaction mechanism for amorphous solid water was summarized as follows:

$$H_2O + h\nu \rightarrow \text{hot-H} + OH,$$

$$\text{HAB: hot-H} + HOH \rightarrow H_2(1500 \text{ K}, 1300 \text{ K}) + OH,$$

$$H_2(1500 \text{ K}, 1300 \text{ K}) \xrightarrow{\text{collision}} H_2(100 \text{ K}, 100 \text{ K}).$$

b. Amorphous solid methanol When CH_3OH is photodissociated, the $H_2(v=0, J=0-2, T_{trans}=100$ K, $T_{rot}=110$ K, 93% contribution) and $H_2(v=0, J=1-5, T_{trans}=2200$ K, $T_{rot}=2500$ K, 7%) are observed. Since the $H_2(v=0)$ products have similar internal energies to those from the photolysis of amorphous solid water, which are formed via the HAB reaction (3), we propose that the $H_2(v=0)$ products from the ASM photolysis are formed via the HAB reactions (9) and (10). The slightly higher temperatures for the $H_2(T_{trans}=2200$ K and $T_{rot}=2500$ K) from ASM than those from amorphous solid water ($T_{trans}=1500$ K and $T_{rot}=1300$ K) come from the fact that reactions (9) and (10) have a smaller standard enthalpy of reaction compared to reaction (3). The HAB reaction mechanism is summarized as follows:

$$CH_3OH + h\nu \rightarrow \text{hot-H} + CH_2OH \text{ or } CH_3O,$$

$$\text{HAB: hot-H} + CH_3OH \rightarrow H_2(2200 \text{ K}, 2500 \text{ K}) + CH_2OH \text{ or } CH_3O,$$

$$H_2(2200 \text{ K}, 2500 \text{ K})$$

TABLE V. Relative populations and translational temperatures of D and H from the photoreactions of solid CD_3OH and translational temperatures of H from the photolysis of amorphous solid water.

	Population ratio		Translational temperature T_{trans} (K) and contribution (%)	$\langle E_{trans} \rangle$ (kcal/mol)
	Total	Nascent[a]		
D from CD_3OH	0.23	0.35	6000 (45%), 700 (10%), 100 (45%)	11.2 ± 1.8
H from CD_3OH	1	1	6000 (30%), 700 (5%), 100 (65%)	7.6 ± 1.3
H from H_2O	–	–	4750 (3%), 625 (5%), 110 (92%)	1.1 ± 0.06

[a]Nascent populations were estimated from the 6000 K components.

$$\xrightarrow{\text{collision}} H_2(100\ \text{K},\ 110\ \text{K}).$$

We found two different vibrational distributions: one peaks at $v=0$ and the other increases with increasing vibrational quantum number for $H_2(v=2-5)$. If vibrational relaxation occurs for $H_2(v=2-5)$, the vibrational population in $v=1$ should be appreciable. In fact its signal intensity was very weak. Similar results were obtained in our previous experiment for H_2 generated from the 157 nm photodissociation of amorphous solid water ice films and support the $H_2(v=0$ and $1)$ formation via the HAB reaction.[3,16]

When CD_3OH is dissociated, the subsequent photoreactions become complicated as follows:

$$\text{UMHE: } CD_3OH \rightarrow CDOH + D_2, \quad (17)$$

$$\text{UMHE: } CD_3OH \rightarrow CD_2O + HD, \quad (18)$$

$$\text{HR: } H + H \rightarrow H_2, \quad (19)$$

$$H + D \rightarrow HD, \quad (20)$$

$$D + D \rightarrow D_2, \quad (21)$$

$$\text{HAB: } H + CD_3OH \rightarrow CD_2OH + HD, \quad (22)$$

$$D + CD_3OH \rightarrow CD_2OH + D_2, \quad (23)$$

$$\text{HAB: } H + CD_3OH \rightarrow CD_3O + H_2, \quad (24)$$

$$D + CD_3OH \rightarrow CD_3 + HD. \quad (25)$$

The thermoneutral abstraction of a hydrogen atom from methanol by the photolytically produced H(D) atom yields translationally and internally cold products via reactions (22)–(25). The relative populations for HD, D_2 and H_2 in the $(v=0,\ J=0)$ level from CD_3OH were 0.60:0.32:0.08. These fractions are reasonable under the assumption that (a) the nascent production ratio of D/H is 0.35, and (b) the HAB mechanism proceeds mostly via reactions (22) and (23) since methyl hydrogen abstraction reaction (9) has the smaller activation energy than hydroxyl hydrogen abstraction reaction (10).

2. Hydrogen molecules in v=2, 3, 4, and 5 levels

a. Amorphous solid water We have previously reported $H_2(v=2,3,4)$ products that had very different translational and internal energy distributions from $H_2(v=0)$ produced via the above-mentioned HAB mechanism for amorphous solid water.[16] The TOF spectra for $H_2(v=3,\ J=3$ and $13)$ were reproduced by two different combinations of MB distributions: $T_{trans}=1800$ K (24%) and 110 K (76%) for $J=3$ and 1800 K (2%) and 110 K (98%) for $J=13$.[3,16] $H_2(v \geq 2,\ T_{trans}=1800\ \text{K})$ products were attributed to the HR mechanism, whereby a photoproduced H atom recombines with a previously adsorbed and thus thermalized H atom trapped close to the ice surface-vacuum interface as schematically shown in Fig. 9(b). The majority of $H_2(v \geq 2)$ were

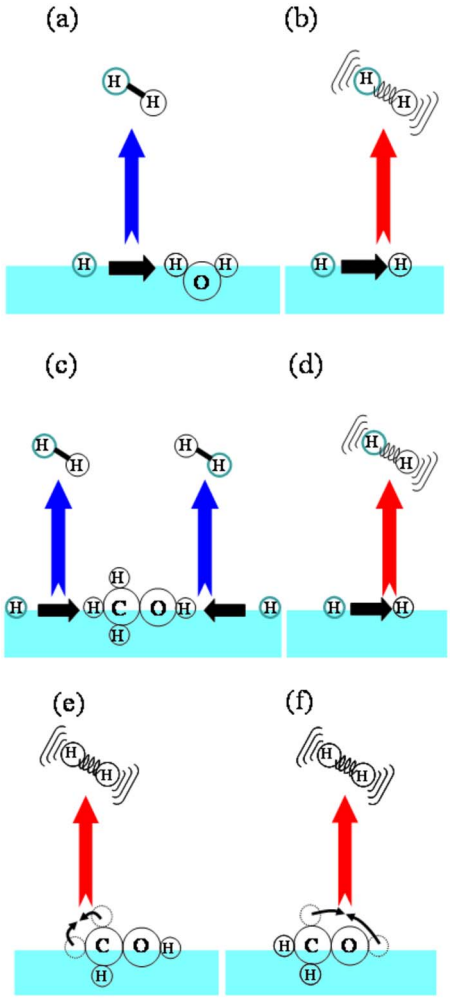

FIG. 9. (Color online) [(a) and (b)] Schematic illustrations for H_2 formation mechanisms following vacuum ultraviolet irradiation of amorphous solid water: (a) $H_2(v=0$ and $1)$ from hydrogen abstraction reaction and (b) $H_2(v \geq 2)$ from hydrogen atom recombination reaction. [(c)–(f)] H_2 from amorphous solid methanol: (c) $H_2(v=0$ and $1)$ from hydrogen abstraction reaction, (d) $H_2(v \geq 2)$ from hydrogen atom recombination reaction, (e) $H_2(v \geq 2)$ from three-center elimination, and (f) $H_2(v \geq 2)$ from four-center elimination.

TABLE VI. Comparison of translational and internal states of H_2 molecules following photolysis of amorphous methanol and amorphous solid water (Ref. 16).

v	Material	Vibrational population ratio [v=2:3:4:5]	Translational temperatures (K)	Averaged energy (kcal/mol)		Major reaction mechanism[a]
				Translational	Rotational	
0	Amorphous solid water		1500 (4%), 100 (96%)	0.6±0.1	0.3±0.04	HAB
	Amorphous solid methanol		2200 (7%), 100 (93%)	1.0±0.1	0.5±0.1	HAB
2, 3, 4, and 5	Amorphous solid water	0.6:1.0:1.3:[b]	1800, 100	0.8±0.3	10.7±2.3	HR
	Amorphous solid methanol	0.4:1.0:1.5:3.4	5000, 1800, 700, 100	7.0±2.4	8.2±2.5	HR and UMHE

[a]HAB: hydrogen atom abstraction mechanism; HR: hydrogen atom recombination mechanism; UMHE: unimolecular hydrogen molecule elimination mechanism.
[b]$H_2(v=5,\ J=1$ and 3) were observed but the relative population was not measured because the signal intensities were weak.

detected with near-thermal translational energies. These $H_2(v\geq 2,\ T_{trans}=110\ K)$ are attributed to the same HR mechanism but occurring in the micropores deeper within the bulk; escape of these H_2 products will involve multiple collisions with the amorphous solid water surface as a result of which their translational energies thermalize to that of the bulk. The main reaction mechanism is summarized as follows:

$$\text{HR: } H + H \rightarrow H_2(v=2,\ 1800\ K),$$

$$H_2(1800\ K) \xrightarrow{\text{collision}} H_2(110\ K).$$

b. Amorphous solid methanol While only the HR reaction occurs for amorphous solid water, both the HR mechanism (2) and the UMHE mechanisms (6) and (7) could occur for ASM. Both processes lead to vibrationally excited $H_2(v=2-5)$ as is schematically illustrated in Figs. 9(d)–9(f),

		ΔH (kcal/mol)	
HR:	$H + H \rightarrow H_2$,	−104	(26)
		E_{avail}(kcal/mol)	
UMHE:	$CH_3OH + h\nu \rightarrow CHOH + H_2$,	110	(27)
UMHE:	$CH_3OH + h\nu \rightarrow CH_2O + H_2$.	162	(28)

The UMHE mechanism is expected to produce H_2 with higher rotational and translational energise compared to the HR mechanism because of large E_{avail}. Table VI shows that $H_2(v=2-5)$ products from ASM have higher translational energy than $H_2(v=2-4)$ from amorphous solid water. The rotational distributions of the H_2 recorded at $t=0.55\ \mu s$ from ASM in Fig. 6 and amorphous solid water in Fig. 3 of Ref. 16 are similar, but the contribution of the higher J levels is larger for ASM, likely because of the contribution of the UMHE mechanism in ASM and its larger excess energy. We calculated the maximum contribution of the HR mechanism for the $H_2(v=3)$ products from CH_3OH to be 40%, assuming that (a) the rotational distribution at $t=0.55\ \mu s$ for amorphous solid water in Fig. 3 of Ref. 16 comes only from the HR reaction and (b) the difference in the rotational distributions at $t=0.55\ \mu s$ between ASM and amorphous solid water in the higher J levels is due only to the UMHE mechanism in ASM. In addition, based on the present experimental results of the molecular hydrogen isotopomers from CD_3OH, the relative population ratio of the $H_2(v=3)$ products that are formed only via HR mechanism is in the range of 6%–20% as shown by the H_2 data in Table IV. Since the nascent atomic production ratio of D/H from CD_3OH is 0.35, the population ratios of H_2:HD:D_2 via the HR mechanism are expected to be 0.55:0.38:0.07. Hence, the contribution of the HR mechanism in the $v=3$ level may be estimated to be $(6\%\sim 20\%)/0.55=11\%\sim 36\%$. Thus, we conclude that D_2 and HD products are mainly formed by the UMHE mechanisms (17) and (18). In addition, the $HD(v=3,\ T_{trans}=5000\ K)$ has larger translational energy than that of $D_2(v=3,\ T_{trans}=1800\ K)$ or $H_2(v=3,\ T_{trans}=1800\ K)$ as shown in Table IV because of the largest excess energy for the UMHE mechanism (18). The reaction mechanisms described above for the UMHE mechanism from ASM are summarized as follows:

$$\text{UMHE: } CD_3OH + h\nu \rightarrow CD_2O + HD(v=2-5,\ 5000\ K),$$

$$HD(5000\ K) \xrightarrow{\text{collision}} HD(700\ K),$$

$$HD(700\ K) \xrightarrow{\text{collision}} HD(100\ K),$$

$$\text{UMHE: } CD_3OH + h\nu \rightarrow CDOH + D_2(v=2-5,\ 1800\ K),$$

$$D_2(1800\ K) \xrightarrow{\text{collision}} D_2(100\ K).$$

The UMHE channel contribution becomes even more dominant when higher vibrational levels of H_2 photoproducts are considered. For example, the TOF spectra (Fig. 4) show that $H_2(v=5)$ products from ASM are formed predominantly with high translational energy ($T_{trans}=5000$ K), and that $H_2(v=5)$ has higher translational energy than the other H_2 products in $v=2$, 3, and 4 (Table II). Since $H_2(T_{trans}=5000\ K)$ is produced mainly via reaction (7), the exothermic UMHE mechanism has more contribution to the formation of $H_2(v=5)$ compared to $H_2(v=2-4)$.

The measured rotational energy distributions of $H_2(v$

≥ 2) from ASM are nonthermal as shown in Fig. 7. The translationally thermalized $H_2(v=3,\ T_{trans}=100\ K)$ is also highly rotationally excited as shown in Fig. 6 and Table III. The persistence of this excitation may be understood with the fact that the quenching probability of $H_2(v,J)$ is reduced as the rotational level spacing increases. This process is not a linear or monotonous process, and for some rotational levels the quasiresonant vibration-rotation (QRVR) relaxation pathways may be important.[29] The general propensity rule for the QRVR relaxation is $E_{rot}(\Delta J=\text{even}) \sim E_{vib}(\Delta v)$. For the $H_2(v \geq 2)$ products, the efficiency of this QRVR pathway shows a local minimum in the range $7 \leq J \leq 12$.[29] On the whole though, the intermediate J levels are quenched readily and regularly into the low J levels whereas the high J levels are not efficiently relaxed because there is no efficient energy receptor state in the ice matrix. As a result, the higher levels retain their significant population and the population distribution among the $J=0-17$ rotational levels cannot be described by a single rotational temperature.

It is difficult to estimate the rate of H_2 formation from photolysis of ASM. However, the rate for amorphous solid water has been estimated to be $\sim 10^{-16}$ cm^{-3} s^{-1} in our previous paper assuming typical parameters in dense clouds, and in warmer ($T > 20$ K) and stronger UV radiation regions this rate would exceed that from recombination of adsorbed H atoms.[3] Andersson and van Dishoeck suggested that the case of a single photon absorption event will be needed to give a realistic picture of photodesorption in dense clouds since the cosmic ray induced UV flux inside dense clouds is small.[30] Since UMHE reaction is a single photon absorption process, it can also yield hydrogen molecule in dense clouds.

C. Ortho/para ratio of H_2 products

The equilibrium ortho-para ratio g_{OPR} for H_2 at 100 K is 1.5 and approaches the statistical limit value, 3, at high temperatures.[26] In all REMPI spectra of H_2 in this study for ASM and also in our previous study on water ice, we found that $g_{OPR}=3$, corresponding to the statistical and high temperature limit. We argue that $g_{OPR}=3$ should be considered the norm for H_2 molecules produced by VUV photolysis of ASM and also water ice by the HR, HAB, and UMHE mechanisms. As for the results of CD_3OH, it is interesting to compare the ratios of H_2 and D_2 in the ortho and para levels, respectively. Table IV shows the relative signal ratios of isotopomers in the various (v,J) levels. In the ortho levels ($J=3$ and 13), the population ratios of D_2 and H_2 are around 0.22 and 0.15, respectively, while in the para levels ($v=3$, $J=14$) those ratios are 0.47 and 0.06. The difference in these relative populations point to different g_{OPR} values for H_2 and D_2, that is, $g_{OPR}=3$ for H_2 and 1/2 for D_2. The measured g_{OPR} values of 2.2 and 0.4 are therefore near the statistical limit values for H_2 and D_2, respectively.

The ortho/para ratio of H_2 is frequently used as an indicator for the physical and chemical history of H_2 formation. The spin temperature is often found to be different from translational and rovibrational temperatures. Ortho-para conversion can occur by spin exchange reactions with protons and ions, but the conversion time scale in space is comparable to the lifetime of typical interstellar molecular clouds. The high temperature value $g_{OPR}=3$ has been widely assumed elsewhere, e.g., in theoretical studies of the HR reaction on an ice surface[8] and in experimental studies of HR on the surface of porous carbon grains.[10–12] We rationalize the use of this same high temperature limiting value by noting that (a) the HR and UMHE reactions are highly exothermic and (b) the HAB reaction is effectively exoergic because of the activation energy for the HAB reaction once past the transition state. In both mechanisms, therefore, any excess energy released during reaction enables g_{OPR} to adopt its high temperature limiting value. These three H_2 formation mechanisms may also be applicable to ice of methane, formaldehyde, ammonia, and hydrated acids that are abundant as interstellar molecules.

V. CONCLUSION

We have investigated the formation mechanisms of hot and cold hydrogen atoms from the vacuum ultraviolet photolysis of ASM at 90 K. Hydrogen molecules in the $v=0-5$ levels are consequently produced by three distinct mechanisms, i.e., (a) HAB from either the methyl or hydroxyl group leading to cold H_2, (b) recombination of H atoms leading to a vibrationally excited H_2, and (c) UMHE reaction leading to even more highly excited H_2 products. Molecular hydrogen formation mechanisms via the hydrogen abstraction and hydrogen recombination reactions are similar to those for the vacuum ultraviolet photolysis of amorphous water ice. The UMHE reaction that yields translationally and rotationally hot $H_2(v=2-5)$ products occurs for ASM but not for amorphous solid ice.

ACKNOWLEDGMENTS

The authors thank Mr. Daisuke Iida for his help in experiments and Professor Naoki Watanabe of Hokkaido University for helpful discussions. This work is supported by a grant-in-aid from JSPS (Grant No. 20245005).

[1] R. J. Gould and E. E. Salpeter, Astrophys. J. **138**, 393 (1963).
[2] G. Manico, G. Raguni, V. Pirronello, J. E. Roser, and G. Vidali, Astrophys. J. **548**, L253 (2001).
[3] A. Yabushita, T. Hama, D. Iida, N. Kawanaka, M. Kawasaki, N. Watanebe, M. N. R. Ashfold, and H.-P. Loock, Astrophys. J. **682**, L69 (2008).
[4] K. M. Pontoppidan, E. Dartois, E. F. van Dishoeck, W. F. Thi, and L. d'Hendecourt, Astron. Astrophys. **404**, L17 (2003).
[5] C. J. Skinner, A. Tielens, M. J. Barlow, and K. Justtanont, Astrophys. J. **399**, L79 (1992).
[6] S. A. Sandford, Meteorit. Planet. Sci. **31**, 449 (1996).
[7] R. A. Sultanov and N. Balakrishnan, Astrophys. J. **629**, 305 (2005).
[8] J. Takahashi, Earth, Planets Space **51**, 1215 (1999).
[9] J. E. Roser, G. Manico, V. Pirronello, and G. Vidali, Astrophys. J. **581**, 276 (2002).
[10] S. C. Creighan, J. S. A. Perry, and S. D. Price, J. Chem. Phys. **124**, 114701 (2006).
[11] F. Islam, E. R. Latimer, and S. D. Price, J. Chem. Phys. **127**, 064701 (2007).
[12] E. R. Latimer, F. Islam, and S. D. Price, Chem. Phys. Lett. **455**, 174 (2008).
[13] A. Kouchi and T. Kuroda, Nature (London) **344**, 134 (1990).
[14] M. S. Westley, R. A. Baragiola, R. E. Johnson, and G. A. Baratta, Nature (London) **373**, 405 (1995).
[15] N. Watanabe, T. Horii, and A. Kouchi, Astrophys. J. **541**, 772 (2000).

[16] A. Yabushita, T. Hama, D. Iida, N. Kawanaka, M. Kawasaki, N. Watanebe, M. N. R. Ashfold, and H.-P. Loock, J. Chem. Phys. **129**, 044501 (2008).
[17] A. Yabushita, D. Kanda, N. Kawanaka, M. Kawasaki, and M. N. R. Ashfold, J. Chem. Phys. **125**, 133406 (2006).
[18] J. T. Jodkowski, M. T. Rayez, J. C. Rayez, T. Berces, and S. Dobe, J. Phys. Chem. A **103**, 3750 (1999).
[19] S. H. Lee, H. I. Lee, and Y. T. Lee, J. Chem. Phys. **121**, 11053 (2004).
[20] P. A. Gerakines, W. A. Schutte, and P. Ehrenfreund, Astron. Astrophys. **312**, 289 (1996).
[21] A. Yabushita, Y. Inoue, T. Senga, M. Kawasaki, and S. Sato, J. Phys. Chem. B **106**, 3151 (2002).
[22] M. Kawasaki, Appl. Surf. Sci. **135**, 115 (1998).
[23] S. M. Dounce, J. Mundy, and H. L. Dai, J. Chem. Phys. **126**, 191111 (2007).
[24] A. Yabushita, Y. Hashikawa, A. Ikeda, M. Kawasaki, and H. Tachikawa, J. Chem. Phys. **120**, 5463 (2004).
[25] A. E. Pomerantz, F. Ausfelder, R. N. Zare, and W. M. Huo, Can. J. Chem. **82**, 723 (2004).
[26] A. Sternberg and D. A. Neufeld, Astrophys. J. **516**, 371 (1999).
[27] S. Andersson, A. Al-Halabi, G. J. Kroes, and E. F. van Dishoeck, J. Chem. Phys. **124**, 064715 (2006).
[28] S. Harich, J. J. Lin, Y. T. Lee, and X. Yang, J. Chem. Phys. **111**, 5 (1999).
[29] E. Bodo and F. A. Gianturco, Int. Rev. Phys. Chem. **25**, 313 (2006).
[30] S. Andersson and E. F. van Dishoeck, Astron. Astrophys. **491**, 907 (2008).